Journal of Medicinal Chemistry

Article

pubs.acs.org/jmc

Tumor-Targeting with Novel Non-Benzoyl 6-Substituted Straight Chain Pyrrolo[2,3-*d*]pyrimidine Antifolates via Cellular Uptake by Folate Receptor α and Inhibition of de Novo Purine Nucleotide Biosynthesis

Yiqiang Wang,[†,⊥,#] Christina Cherian,[‡,§,#] Steven Orr,[‡,§] Shermaine Mitchell-Ryan,[§] Zhanjun Hou,[‡,§] Sudhir Raghavan,[†] Larry H. Matherly,[*,‡,§,∥,#] and Aleem Gangjee[*,†,#]

[†]Division of Medicinal Chemistry, Graduate School of Pharmaceutical Sciences, Duquesne University, 600 Forbes Avenue, Pittsburgh, Pennsylvania 15282, United States

[‡]Molecular Therapeutics Program, Barbara Ann Karmanos Cancer Institute, 110 East Warren Avenue, Detroit, Michigan 48201, United States

[§]Department of Oncology, Wayne State University School of Medicine, Detroit, Michigan 48201, United States

[∥]Department of Pharmacology, Wayne State University School of Medicine, Detroit, Michigan 48201, United States

Supporting Information

ABSTRACT: A new series of 6-substituted straight side chain pyrrolo[2,3-*d*]pyrimidines **3a−d** with varying chain lengths (n = 5−8) was designed and synthesized as part of our program to provide targeted antitumor agents with folate receptor (FR) cellular uptake specificity and glycinamide ribonucleotide formyltransferase (GARFTase) inhibition. Carboxylic acids **4a−d** were converted to the acid chlorides and reacted with diazomethane, followed by 48% HBr to generate the α-bromomethylketones **5a−d**. Condensation of 2,4-diamino-6-hydroxypyrimidine **6** with **5a−d** afforded the 6-substituted pyrrolo[2,3-*d*]pyrimidines **7a−d**. Hydrolysis and subsequent coupling with diethyl L-glutamate and saponification afforded target compounds **3a−d**. Compounds **3b−d** showed selective cellular uptake via FRα and -β, associated with high affinity binding and inhibition of de novo purine nucleotide biosynthesis via GARFTase, resulting in potent inhibition against FR-expressing Chinese hamster cells and human KB tumor cells in culture. Our studies establish, for the first time, that a side chain benzoyl group is not essential for tumor-selective drug uptake by FRα.

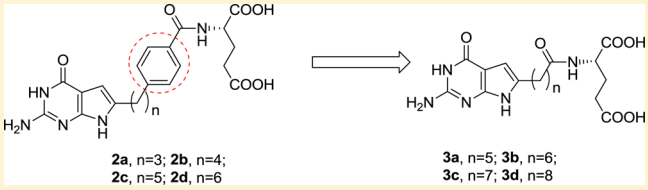

INTRODUCTION

Folates are essential for cell growth and tissue regeneration. Membrane transport of extracellular folates is required because mammalian cells cannot synthesize folates de novo. Three major folate uptake systems have been reported.[1−5] (i) The reduced folate carrier (RFC or SLC19A1) is an anion antiporter that is ubiquitously expressed in tissues and tumors and is the major membrane transport system for folates in mammalian cells at physiologic pH.[1] (ii) Folate receptors (FRs) α and β are glycosyl phosphatidylinositol-anchored proteins that mediate cellular uptake of folates by receptor-mediated endocytosis.[2,3] High levels of FRs are expressed in a number of malignancies, including ovarian and endometrial cancers (FRα) and in myeloid leukemias (FRβ).[2,3] However, FRs show a more restricted tissue distribution than RFC. In normal tissues where they are expressed, FRs are either inaccessible to circulating folate cofactors (FRα in renal tubules) or are nonfunctional (FRβ in normal hematopoietic cells).[2,3] (iii) The proton-coupled folate transporter (PCFT; SLC46A1) is a recently discovered proton-folate symporter that functions optimally at acidic pH by coupling the downhill flow of protons to the uphill transport of folates.[4,5] PCFT is widely expressed in human solid tumors[4] and in modest levels in most normal tissues, although high levels of PCFT are present in the duodenum and jejunum, as well as in the liver and kidney.[5]

Folate-dependent biosynthetic pathways are important therapeutic targets for cancer chemotherapy.[6−8] Clinically relevant antifolate drugs for cancer include potent inhibitors of dihydrofolate reductase [methotrexate (MTX), pralatrexate (PDX)], thymidylate synthase [raltitrexed (RTX), pemetrexed (PMX)], and the purine nucleotide biosynthetic enzymes, β-glycinamide ribonucleotide (GAR) formyltransferase (GARFTase) [PMX] and 5-aminoimidazole-4-carboxamide (AICA) ribonucleotide formyltransferase (AICARFTase) [PMX][6−8] (Figure 1). Although all these agents are transported by RFC,[1,9] the expression of RFC in both normal and tumor cells presents a potential obstacle to antitumor selectivity. Further, loss of RFC is frequently associated with antifolate resistance.[1,8,10] Thus, it is of interest to design tumor-targeted antifolates that are specific substrates for transporters other than RFC with limited expression and/or transport into normal tissues compared with tumors. If these drugs also inhibit targets other than dihydrofolate

Received: July 26, 2013
Published: October 10, 2013

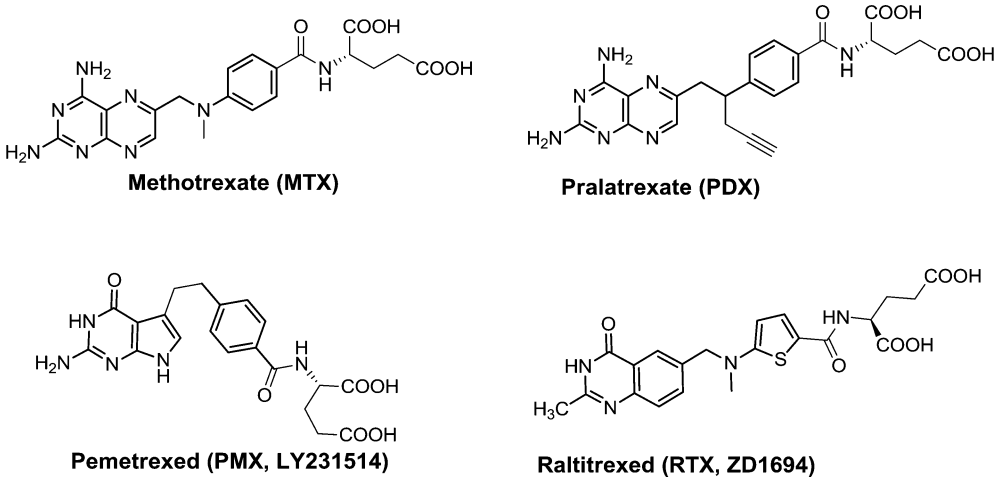

Figure 1. Structures of clinically relevant antifolates transported by RFC.

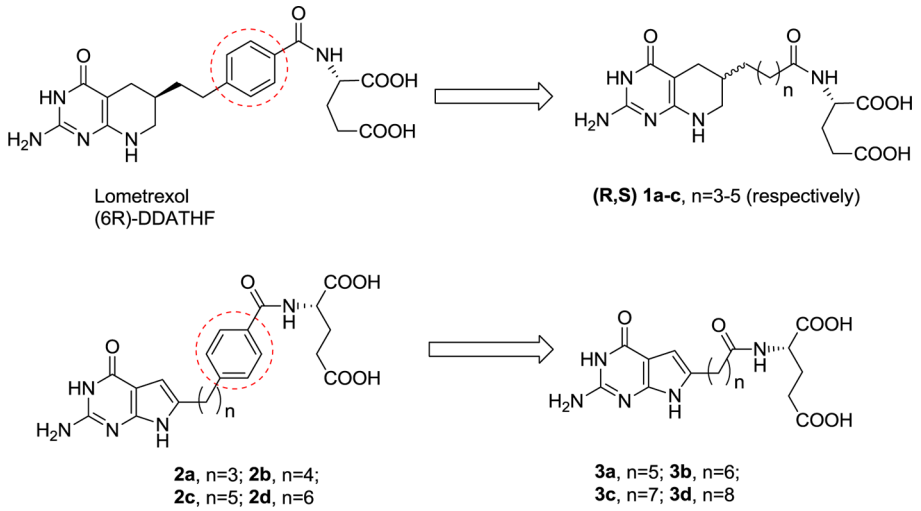

Figure 2. 6-Substituted non-benzoyl straight chain compounds **3a−d**, based on lometrexol (LMTX) and compounds **1a−c**, showing replacement of the phenyl ring in compounds **2a−2b** by 2−5 methylene groups.

reductase and thymidylate synthase, this would afford further benefit by circumventing resistance due to increased levels or mutated forms of these enzyme targets. This reasoning was a major impetus to develop novel agents with selective uptake into tumors by FRs or PCFT over RFC and which specifically target de novo purine nucleotide biosynthesis.[5,6,11−16]

We previously reported a series of 6-substituted pyrrolo[2,3-*d*]-pyrimidine phenyl antifolates **2a−d**.[11,13] (Figure 2) A highly active compound of this series was the 3-carbon bridge analog (**2a**) which was a targeted agent selectively transported into certain tumor cells by FRs and PCFT but not RFC.[11,13] Once intracellular, compound **2a** inhibited GARFTase in de novo purine nucleotide biosynthesis, resulting in depletion of purine nucleotides.[11,13] Further, compound **2a** was highly active in vitro toward both KB and IGROV1 tumors.[11] To further explore the structure−activity relationships (SAR) for GARFTase inhibition and non-RFC targeted transport specificity, we synthesized and tested several series of related analogues with modifications of the aromatic rings and aliphatic linkers.[5,6,12−16]

Lometrexol (LMTX) is an early generation GARFTase inhibitor[17] that was tested in a phase I clinical trial and was found to be unacceptably toxic.[18] This failure was likely due, at least in part, to its membrane transport into normal cells by RFC. A series of LMTX analogues, **1a−c**, was reported in which the phenyl ring in the bridge was replaced by a methylene bridge of variable length[19,20] (Figure 2). Interestingly, replacement of the phenyl ring of LMTX by two, three, or four carbon atom chains substantially preserved both binding to GARFTase[19] and polyglutamylation by folylpolyglutamate synthetase (FPGS).[20] However, these analogues were not tested for their membrane transport by the major folate transporters or for their capacities to inhibit cell proliferation.

In the present work, we designed an analogous series of 6-substituted pyrrolo[2,3-*d*]pyrimidine analogues to examine the impact of an alkyl-for-benzoyl ring replacement on folate transporter specificity, GARFTase inhibition, and antiproliferative activities. Straight chain compounds **3a−d** were designed with replacement of the phenyl ring of the lead compound **2a** by a methylene bridge of variable length (n = 2−5) (Figure 2). The precursor acids, **7e−h** (Scheme 1), were also biologically evaluated to determine the importance of the L-glutamate moiety to their biological effects. Collectively, our results establish that aliphatic replacement of the benzoyl ring in the 6-substituted pyrrolo[2,3-*d*]pyrimidine series preserves substantial selective FR-directed cellular uptake and GARFTase inhibition, with potent inhibition of tumor cell proliferation, as long as there is

dx.doi.org/10.1021/jm401139z | J. Med. Chem. 2013, 56, 8684−8695

Scheme 1

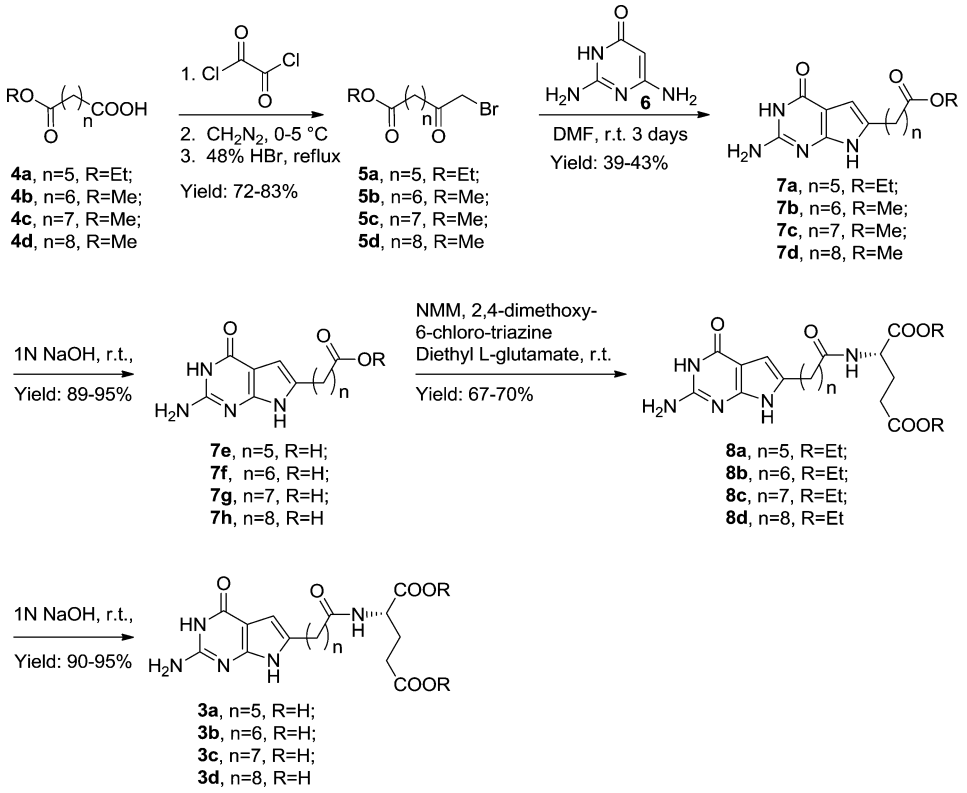

4a, n=5, R=Et;
4b, n=6, R=Me;
4c, n=7, R=Me;
4d, n=8, R=Me

5a, n=5, R=Et;
5b, n=6, R=Me;
5c, n=7, R=Me;
5d, n=8, R=Me

7a, n=5, R=Et;
7b, n=6, R=Me;
7c, n=7, R=Me;
7d, n=8, R=Me

7e, n=5, R=H;
7f, n=6, R=H;
7g, n=7, R=H;
7h, n=8, R=H

8a, n=5, R=Et;
8b, n=6, R=Et;
8c, n=7, R=Et;
8d, n=8, R=Et

3a, n=5, R=H;
3b, n=6, R=H;
3c, n=7, R=H;
3d, n=8, R=H

sufficient distance between the bicyclic ring system and the terminal L-glutamate.

CHEMISTRY

Compounds **3a−d** (n = 5−8) were synthesized using an α-bromomethyl ketone condensation with 2,4-diamino-4-oxo-pyrimidine **6** as the key step outlined in Scheme 1. Commercially available carboxylic acids **4a−d** were converted to the acid chlorides and immediately reacted with diazomethane, followed by 48% HBr to give the desired α-bromomethylketones **5a−d**.[11] Condensation of 2,4-diamino-6-hydroxypyrimidine **6** with **5a−d** afforded the 6-substituted pyrrolo[2,3-*d*]pyrimidines **7a−d**. Hydrolysis of **7a−d** afforded **7e−h**. Subsequent coupling with diethyl L-glutamate using *N*-methyl morpholine and 2,4-dimethoxy-6-chlorotriazine as the activating agents afforded the diesters **8a−d**. Final saponification of the diesters gave the target compounds **3a−d** (n = 5−8).

BIOLOGICAL EVALUATION AND DISCUSSION

Non-benzoyl 6-Carbon Chain Pyrrolo[2,3-*d*]pyrimidine Antifolates Are Inhibitors of Cell Proliferation, Correlating with Expression of Folate Receptors. Our goal was to examine the role of the side chain phenyl ring and the terminal L-glutamate of the pyrrolo[2,3-*d*]pyrimidine antifolates as determinants of folate transporter selectivity, GARFTase inhibitory activity, and antiproliferative activity based on prior studies of compounds **2a−d**. We previously showed that the intramolecular distance between the bicyclic scaffold and the L-glutamate moiety of the latter series was an important determinant of inhibitory potency toward FR-expressing cell lines,[10,11,13−15] so this was also examined.

Compounds **3a−d** (Figure 2) and **7e−h** (Scheme 1) were tested in cell proliferation assays with a well-characterized cohort of isogenic Chinese hamster ovary (CHO) sublines previously engineered to individually express the major (anti)folate cellular uptake systems including RFC (PC43-10),[21] FRα and β (RT16 and D4, respectively),[11] or PCFT (R2/PCFT4).[12,13] Additional testing was performed with KB human nasopharyngeal carcinoma cells which express RFC, FRα, and PCFT.[11,12] Experiments were performed in standard RPMI 1640/10% dialyzed fetal bovine serum (dFBS) (PC43-10) and in folate-defined media {folate-free RPMI1640/10% dFBS, supplemented with 2 nM (RT16, D4, KB) or 25 nM leucovorin [(6*R*,*S*)5-formyl tetrahydrofolate (LCV)] (R2/PCFT4)}. The impact of the drug treatments on cell proliferation was measured after 96 h, and results were compared to negative controls including RFC-, FR-, and PCFT-null MTXRIIOua^{R}2−4 (R2) CHO cells[11,12,21] [either the parental R2 subline or vector control R2(VC) cells]. For FR-expressing CHO and KB cells, parallel cultures were treated with drugs along with excess folic acid (200 nM) to block drug binding and cellular uptake by FRs. Internalization of exogenous folic acid by FRs would also increase intracellular folate pools. Results were compared with those for the lead 6-substituted pyrrolo[2,3-*d*]pyrimidine benzoyl analogues **2a−d** and are summarized in Table 1.

The data in Table 1 clearly establish that the compounds (**7e−h**) lacking the L-glutamate are not inhibitory, regardless of the cell line model tested. Compounds **3a−d** were also inactive up to 1000 nM toward RFC-expressing PC43-10 cells and PCFT-expressing R2/PCFT4 CHO cells. Compounds **3a−d** were inhibitory toward CHO cells engineered to express FRα and FRβ, as well as FRα-expressing KB tumor cells. Growth inhibition was abolished in the presence of excess (200 nM) folic acid. The most potent inhibitor was **3c** (7-carbon atom chain), followed by **3d** (8-carbon chain) and **3b** (6-carbon chain). The 5-carbon chain analogue, **3a**, was a much poorer inhibitor of cell

dx.doi.org/10.1021/jm401139z | J. Med. Chem. 2013, 56, 8684−8695

Table 1. IC_{50}s (in nM) for 6-Substituted Pyrrolo[2,3-*d*]pyrimidine Antifolates and Classical Antifolates in RFC-, PCFT-, and FR-Expressing Cell Lines[a]

	hRFC		hFRα		hFRβ		hPCFT		hRFC/FRα/hPCFT	
antifolate	PC43-10	R2	RT16	RT16 (+FA)	D4	D4 (+FA)	R2/hPCFT4	R2(VC)	KB	KB (+FA)
2a	648.6(38.1)	>1000	4.1(1.6)	>1000	5.6(1.2)	>1000	23.0(3.3)	>1000	1.7(0.4)	>1000
2b	>1000	>1000	6.3(1.6)	>1000	10(2)	>1000	213(28)	>1000	1.9(0.7)	>1000
2c	>1000	>1000	54(21)	>1000	80(9)	>1000	>1000	>1000	13(7.2)	>1000
2d	>1000	>1000	162(18)	>1000	198(34)	>1000	>1000	>1000	23(12)	>1000
7e	>1000	>1000	>1000	>1000	>1000	>1000	>1000	>1000	>1000	>1000
7f	>1000	>1000	>1000	>1000	>1000	>1000	>1000	>1000	>1000	>1000
7g	>1000	>1000	>1000	>1000	>1000	>1000	>1000	>1000	>1000	>1000
7h	>1000	>1000	>10000	>100	>1000	>1000	>1000	>1000	>1000	>1000
3a	>1000	>1000	>1000	>1000	214(62)	>1000	>1000	>1000	200.3(34.6)	>1000
3b	>1000	>1000	47.1(16.5)	>1000	10.55(3.69)	>1000	>1000	>1000	7.9 (0.72)	>1000
3c	>1000	>1000	8.54(1.53)	>1000	0.87(0.12)	>1000	>1000	>1000	1.10(0.88)	>1000
3d	>1000	>1000	12.31 (3.14)	>10000	3.99(0.57)	>1000	>1000	>1000	1.48(0.04)	>1000
LMTX	12(2.3)	>1000	12(8)	188(41)	2.6(1.0)	275(101)	38.0(5.3)	>1000	1.2(0.6)	31(7)
MTX	12(1.1)	216(8.7)	114(31)	461(62)	106(11)	211(43)	121(17)	>1000	6.0(0.6)	20(2.4)
PDX	0.69(0.07)	819(94)	168(50)	>1000	ND	ND	57(12)	>1000	0.47(0.20)	1.94(0.28)
PMX	138(13)	894(93)	42(9)	388(68)	60(8)	254(78)	13.2(2.4)	974.0(18.1)	68(12)	327(103)
RTX	6.3(1.3)	>1000	15(5)	>1000	22(10)	746(138)	99.5(11.4)	>1000	5.9(2.2)	22(5)

[a]Growth inhibition assays were performed for CHO sublines engineered to express human RFC (PC43-10), FRs α and β (RT16 and D4, respectively), or PCFT (R2/PCFT4), for comparison with transporter-null [R2, R2(VC)] CHO cells and for the KB human tumor subline (expresses RFC, FRα, and PCFT), as described in the Experimental Section. For the FR experiments, growth inhibition assays were performed in the presence and the absence of 200 nM folic acid (FA). The data shown are mean values from 3−10 experiments (plus/minus SEM in parentheses). Results are presented as IC_{50} values, corresponding to the concentrations that inhibit growth by 50% relative to cells incubated without drug. Data for MTX, PMX, RTX, and LMTX and for compounds **2a−d** were previously published.[11,13] The structures for the classical antifolate drugs are shown in Figure 1 and those for compounds **7e−h** and **3a−d** are shown in Figure 2 and Scheme 1. ND: not determined.

proliferation. Growth inhibitions, as reflected in the IC_{50} values, were similar with FRα-expressing sublines (KB, RT16) for compounds **2a**, **2b**, **3c**, and **3d**. Whereas sensitivities of FRα-expressing RT16 cells were similar to those for FRβ-expressing D4 cells for compounds **2a** and **2b**, D4 cells were distinctly more sensitive to the non-benzoyl compounds **3b−3d**. The FR specificity for the active analogues of this series contrasts with results with classic antifolates including MTX, RTX, PMX, PDX, and LMTX, for which antiproliferative activities for RFC- and PCFT-expressing cells exceeded those for FR-expressing cells (Table 1).

Binding of Non-Benzoyl Pyrrolo[2,3-*d*]pyrimidine Antifolates to FRα and β. Compounds **3a−d** are all inhibitors of proliferation for cell lines that express FRα (RT16, KB) and FRβ (D4) (Table 1). The inhibitory effects of these active compounds were blocked by excess folic acid, consistent with their surface binding and internalization by FRs.

Surface FR binding of cytotoxic folate analogues is an essential step for drug internalization by this mechanism and for inhibition of intracellular enzyme targets.[11,12,14−16] To establish a SAR for FRα and -β binding of this series, in particular the impact of alkyl chain length (5−8 carbons) for the 6-substituted analogues and of the terminal L-glutamate on FR binding, we performed competitive binding assays with compounds **3a−d** and **7e−h** at pH 7.4. In these experiments, unlabeled pyrrolo[2,3-*d*]-pyrimidine compounds were tested for their abilities to compete for surface FR binding with [^{3}H]folic acid. FR binding of unknown ligands was compared to those for positive (compounds **2a** and **2b**, also folic acid) and negative (MTX) controls, with documented FR-binding characteristics. The CHO sublines expressing FRα (RT16) or FRβ (D4) were initially rinsed with acid-buffered saline to release FR-bound folates, followed by incubation with [^{3}H]folic acid (at pH 7.4) in the presence of unlabeled (anti)folate competitors over a range of concentrations.[11,12,14−16] After further washing the cells (pH 7.4), FR-bound [^{3}H]folic acid was quantitated and normalized to cell protein and results calculated as pmol [^{3}H]folic acid bound to FRs per mg cell protein. Relative affinities were expressed as inverse molar ratios of (anti)folates required to decrease bound [^{3}H]folic acid by 50% normalized to the affinity for unlabeled folic acid in each experiment (assigned a value of 1.0).[11,12,14−16] The results are expressed as mean values ± standard errors and are presented in Figure 3.

With the 6-substituted analogues that included terminal L-glutamates (**3a−d**), FR binding increased with increasing substituent chain length (**3d** > **3c** > **3b** > **3a**) for both FRα and -β, with compound **3d** exhibiting relative binding affinities approximating those for compounds **2a** and **2b** and slightly less than for folic acid (Figure 3). The lack of a terminal L-glutamate (compounds **7e−h**) had a deleterious effect on FR binding, consistent with the results for the cell proliferation experiments (Table 1). For FRα (but not FRβ), compound **7h** with the 8-carbon chain showed detectable binding. Interestingly, binding of the active linear analogues (compounds **3b**, **3c**, and **3d**) was consistently reduced for FRβ compared to FRα in spite of their increased antiproliferative effects toward FRβ-expressing D4 cells over FRα-expressing RT16 cells (Table 1).

These results demonstrate that the presence of a phenyl side chain ring system for the 6-substituted pyrrolo[2,3-*d*]pyrimidine analogues is not obligatory for binding to FRα or -β. Further, whereas FR binding is clearly critical to cellular uptake of cytotoxic folate analogues, this parameter shows at best an inexact correlation with antiproliferative activities of the non-benzoyl pyrrolo[2,3-*d*]pyrimidine series of analogues. Nonetheless, FR binding for both FR α and -β was greatest for the compounds (**3c** and **3d**) with the most potent antiproliferative effects.

dx.doi.org/10.1021/jm401139z | J. Med. Chem. 2013, 56, 8684−8695

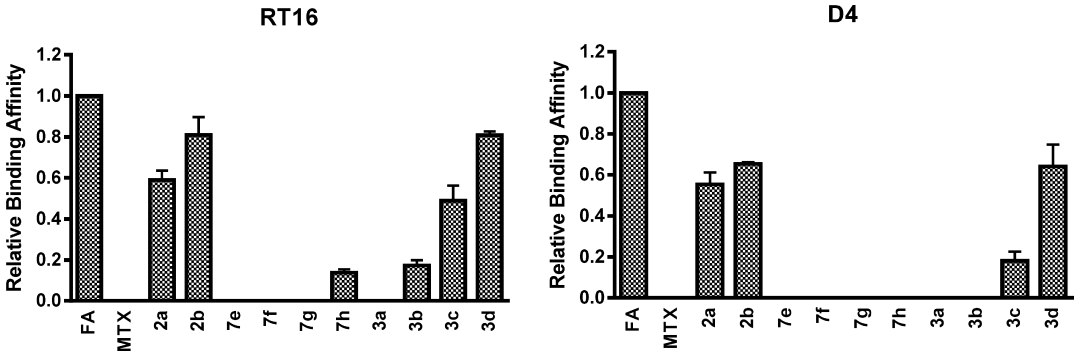

Figure 3. Binding of non-benzoyl 6-substituted pyrrolo[2,3-*d*]pyrimidine analogues (**3a−d** and **7e−h**) to FRα (RT16) and FRβ (D4), compared to compounds **2a** and **2b**. Data are shown for the effects of the unlabeled ligands with FRα-expressing RT16 and FRβ-expressing D4 CHO cells. Binding affinities for assorted folate/antifolate substrates were determined over a range of ligand concentrations and were calculated as the inverse molar ratios of unlabeled ligands required to inhibit [^{3}H]folic acid binding by 50%. Relative binding affinities for individual experiments were normalized to that for unlabeled folic acid which was assigned a value of 1.0. For the various ligands, results are presented as mean values ± standard errors from three experiments. Details for the binding assays are provided in the Experimental Section. Undefined abbreviations: FA, folic acid. The results for compounds **2a** and **2b** were previously published.[11]

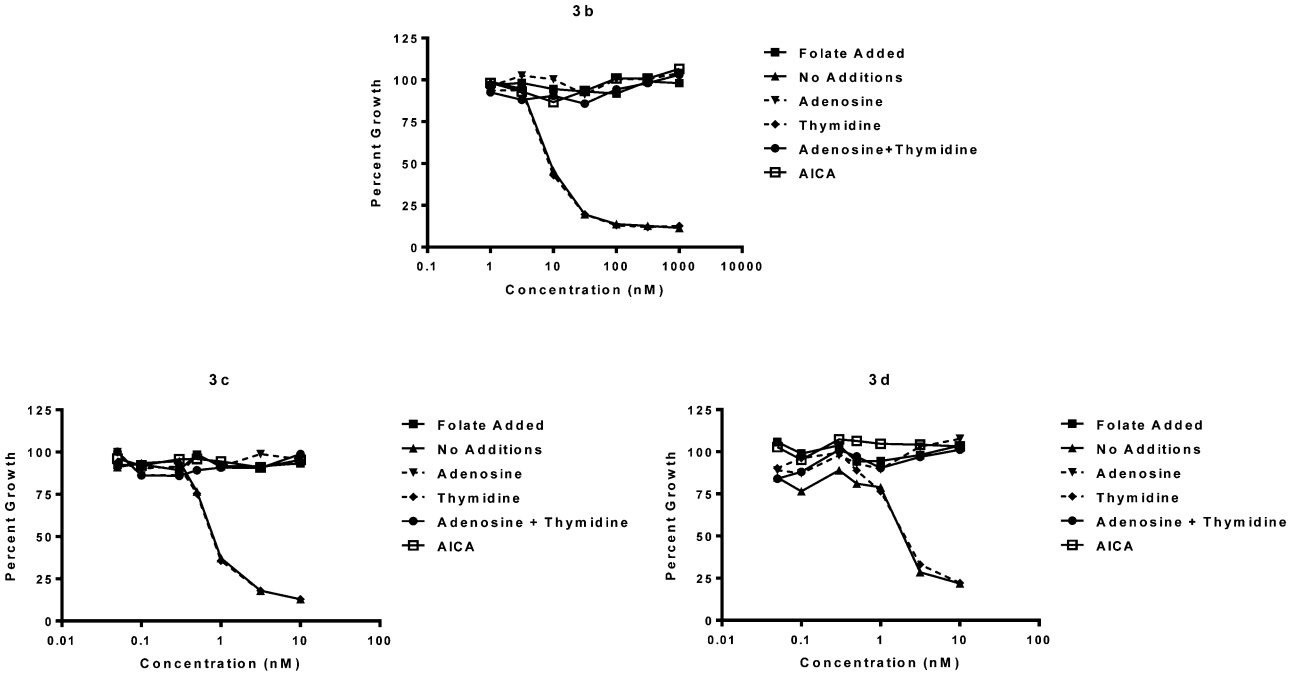

Figure 4. Protection of KB cells from growth inhibition by non-benzoyl 6-substituted pyrrolo[2,3-*d*]pyrimidine analogues **3b−d** in the presence of nucleosides and 5-aminoimidazole-4-carboxamide (AICA). Proliferation inhibition was measured for KB cells over a range of concentrations of compounds **3b−d**, as shown, in complete folate-free RPMI1640 with 2 nM LCV in the absence of other additions (labeled "No Additions"), or in the presence of 200 nM folic acid (labeled "Folate Added"), adenosine (60 μM), thymidine (10 μM), adenosine plus thymidine, or AICA (320 μM). Cell densities were measured with CellTiter Blue fluorescence dye and a fluorescence plate reader. Results were normalized to cell densities in the absence of drug. Results shown are representative data of experiments performed in triplicate.

Determination that GARFTase Is the Major Cellular Target for Compounds 3b, 3c, and 3d. Previous reports of non-benzoyl analogues of LMTX, **1a−c**, in which the phenyl ring was replaced by 2−4 methylene groups (Figure 2), established that the aromatic B ring is not essential for binding to the GARFTase active site, as these novel antifolate compounds were potently inhibitory toward purified murine GARFTase.[19] Further, compounds **1a−c** were all excellent substrates for polyglutamylation by murine FPGS.[20]

By analogy to compounds **1a−c** and the parent 6-substituted pyrrolo[2,3-*d*]pyrimidines **2a** and **2b**, we hypothesized that the non-benzoyl analogues **3b−d** were also GARFTase inhibitors. To establish the targeted pathway for compounds **3b−d** (i.e., de novo thymidylate versus de novo purine nucleotide biosynthesis), exogenous thymidine and adenosine were tested for their capacities to reverse their growth inhibitory effects toward KB cells (Figure 4).[11−17] AICA, a precursor of the AICARFTase substrate was added to circumvent the step catalyzed by GARFTase so as to distinguish inhibition of GARFTase from AICARFTase.[11−17]

For non-benzoyl pyrrolo[2,3-*d*]pyrimidine analogues **3b−d**, thymidine (10 μM) had no impact on the extent of inhibition of cell proliferation, indicating that thymidylate biosynthesis (i.e., thymidylate synthase) was not being targeted. Conversely,

dx.doi.org/10.1021/jm401139z | J. Med. Chem. 2013, 56, 8684−8695

both adenosine (60 μM) and AICA (320 μM) completely reversed the inhibitory effects of this series, establishing that de novo purine nucleotide biosynthesis in general and GARFTase in particular were the likely intracellular targets (Figure 4). Essentially identical results were previously published for compounds **2a** and **2b**.[11] In addition, in experiments with recombinant DHFR and TS, compounds **3b−3d** were not inhibitory (data not shown).

We used an in situ activity assay to *directly* measure cellular GARFTase activity in KB cells treated with the novel antifolates.[11−17] Cells were incubated with [^{14}C]glycine as a radiotracer for 15 h in the presence of compounds **3b−d** under conditions and at concentrations approximating those used in the cell proliferation experiments (Table 1). In this metabolic assay, [^{14}C]glycine is incorporated into the GARFTase substrate [^{14}C]GAR and subsequently into [^{14}C]formyl GAR (by GARFTase), which accumulates in the presence of azaserine. Following protein precipitation with trichloroacetic acid, the acid-soluble metabolites are extracted and fractionated by ion-exchange chromatography, permitting quantitation of [^{14}C]formyl GAR normalized to cellular protein.

The results show that in KB cells, compounds **3b−d** were all potent GARFTase inhibitors at extracellular drug concentrations approximating those required to inhibit cell proliferation

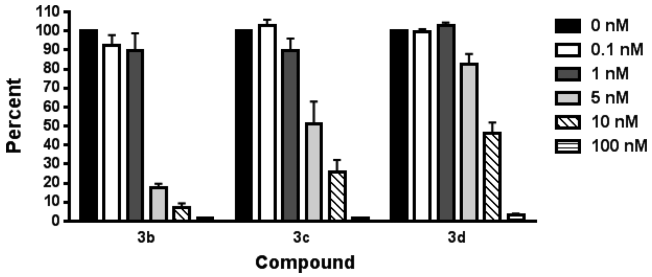

Figure 5. In situ GARFTase inhibition assay. For the in situ assays, incorporation of [^{14}C]glycine into [^{14}C]formyl GAR was measured in KB tumor cells cultured for 15 h in complete folate-free RPMI 1640 plus 2 nM LCV. Details are described in the Experimental Section. Results are presented as a percent of control treated without drugs for KB cells treated with nanomolar concentrations of **3b−d**. Results are presented as mean IC_{50} values ± standard errors. Mean IC_{50}s (± SEs) were calculated as 2.89 (± 0.62) nM for **3b**, 5.49 (± 1.36) nM for **3c**, and 9.62 (± 0.98) nM for **3d**. For comparison, IC_{50}s for compounds **2a** and **2b** were 18 (± 2) nM and 6.8 (± 0.9) nM, respectively.[11]

(Figure 5). Calculated IC_{50} values for GARFTase inhibition varied within a 3-fold range from 2.89 for compound **3b** to 9.62 nM for compound **3d**. By comparison, the IC_{50}s for the 3- and 4-carbon benzoyl analogues **2a** and **2b** were 18 and 6.8 nM, respectively.[11]

These results unambiguously demonstrate that the absence of a side chain benzoyl ring system in the 6-substituted pyrrolo[2,3-*d*]-pyrimidine series is not required to potently inhibit intracellular GARFTase, analogous to results for the non-benzoyl analogues of LMTX **1a−c** (Figure 1).

Molecular Modeling: Docking Studies of Compound 3c with Human GARFTase. Figure 6 shows the docked pose of **3c** (n = 7) in the human GARFTase (PDB ID: 1NJS)[22] active site. The cofactor binding pocket of GARFTase is located at the interface between the N-terminal mononucleotide binding domain and the C-terminal half of the structure. The binding site for the folate cofactor moiety consists of three parts: the pteridine binding cleft, the benzoylglutamate region, and the formyl transfer region.[22] The docked pose shows the pyrrolo[2,3-*d*]pyrimidine scaffold of **3c** to be buried deep in the active site and occupies the same location as the diaminopyrimidine ring in the native crystal structure ligand 10-trifluoroacetyl-5,10-dideaza-acyclic-5,6,7,8-tetrahydrofolic acid (10-CF_3CO-DDACTHF). This orientation of the scaffold permits the 2-amino moiety of **3c** to form hydrogen bonds to Glu141 and the backbone of Leu92. The N1 nitrogen interacts with the backbone of Leu92 to form a hydrogen bond. The 4-oxo moiety forms a hydrogen bond with Asp144 and forms water-mediated hydrogen bonds with Asp142 and Ala140. The molecule is oriented in a manner that aids the N7-nitrogen to form a hydrogen bond with Arg90. As is shown with 10-CF_3CO-DDACTHF (Figure 6), several hydrophobic residues flank the pocket which holds the pyrrolo[2,3-*d*]pyrimidine scaffold. The hydrophobic pocket consists of Leu85, Ile91, Leu92, Val97 (not shown), and the folate binding loop residues 141−146. The amide NH of the L-glutamate forms a hydrogen bond with Met89. The 7-carbon side chain of **3c** shifts the glutamate side chain away from the corresponding glutamate side chain of 10-CF_3CO-DDACTHF. The carbonyl group of the glutamate side chain of **3c** interacts with Arg64, which is not seen with the corresponding carbonyl group of the side chain of 10-CF_3CO-DDACTHF. The γ-carboxylic acid of **3c** interacts with Arg64. The α-carboxylic acid of the glutamate side chain of **3c** interacts with Arg90. Thus, the interaction pattern of the α- and γ-carboxylic acid moieties of **3c** are reversed compared

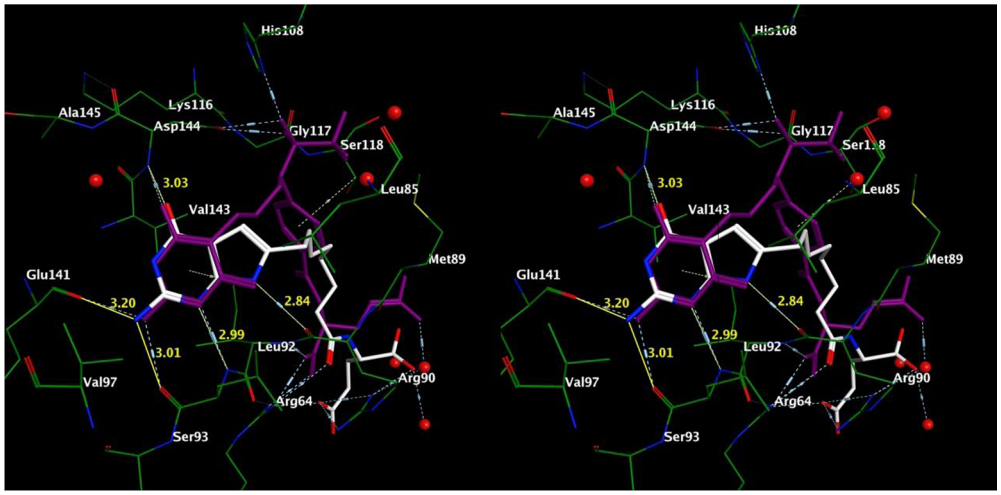

Figure 6. Stereoview overlay of the docked pose of **3c** (white) with 10-CF_3CO-DDACTHF (purple) in human GARFTase (PDB ID: 1NJS).[22]

dx.doi.org/10.1021/jm401139z | J. Med. Chem. 2013, 56, 8684−8695

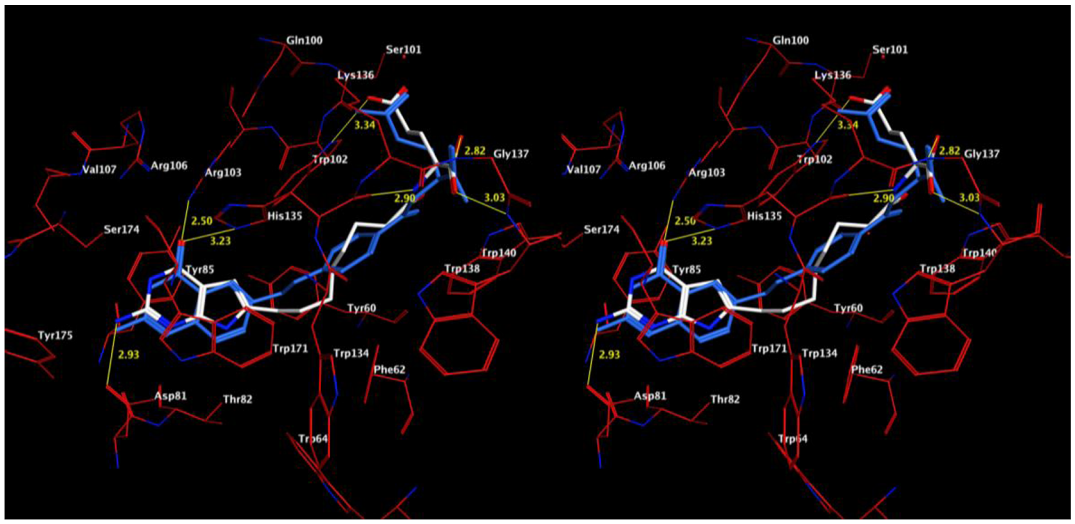

Figure 7. Stereoview overlay of the docked pose of compound **3c** (white) with folic acid (blue) in human FRα (PDB ID: 4LRH).[23]

to the corresponding α- and γ-carboxylic acids of 10-CF_3CO-DDACTHF and could represent an alternate conformation of the side chain. These interactions could easily permit binding and potent inhibition of **3c** against GARFTase, as demonstrated by the results of our in situ GARFTase assays (Figure 5).

Molecular Modeling: Docking Studies of Compound 3c with Human FRα. The X-ray crystal structure of human FRα with folic acid was recently published.[23] Accordingly, we determined the docked structure of **3c** (a prototype of the non-benzoyl series of 6-substituted pyrrolo-[2,3-*d*]pyrimidine analogues) with FRα.

Figure 7 shows the docked pose of compound **3c** in the human FRα (PDB ID: 4LRH)[23] binding site. The long and open folate-binding pocket of FRα contains a predominantly negatively charged pocket where the pteroate group of folic acid binds and a positively charged entrance of the binding pocket which is occupied by the glutamate moiety of folic acid. In its docked pose, the pyrrolo[2,3-*d*]pyrimidine scaffold of **3c** binds similar to the pterin scaffold of folic acid. The 2-NH_2 moiety of **3c** interacts with the side chain carboxylic acid of Asp81. Additional hydrogen bonds are formed between N3 and the side chain hydroxyl of Ser174 and between the 4-oxo group and the side chain NH of Arg103 and His135. The pyrrolo[2,3-*d*]pyrimidine scaffold is sandwiched between the side chains of Tyr60 and Tyr171, similar to the pteridine ring seen in the bound conformation of folic acid. The pyrrole NH of **3c** does not interact with the binding pocket. The flexible C6-substituted chain in **3c** enables the glutamate moiety to be oriented similarly to the corresponding groups in folic acid. The α-carboxylic acid of **3c** can form hydrogen bonds with the backbone NH of Gly137 and Trp138, while the γ-carboxylic acid interacts with the backbone NH of Lys136 and the side chain NH of Trp102. The hydrophobic C6-linker of **3c** can interact in the linker region with surrounding hydrophobic amino acids such as Tyr60, Phe62, Trp102, Trp134, and His135. The docking score of **3c** with FRα was −46.4850.

CONCLUSIONS

There is growing interest in tumor targeting of cytotoxic folate-based therapeutics via their selective cellular uptake by FRs or PCFT over RFC.[5,6,11−16] Specific uptake by FRs or PCFT but not RFC would afford these analogues selectivity for tumor cells expressing FRα and -β and/or PCFT and significant advantages over classical antifolates such as RTX or PMX that are transported by all systems.[1,5]

In previous studies, we began establishing a SAR for FR and PCFT binding and cellular uptake vis á vis RFC and of GARFTase inhibition in de novo purine nucleotide biosynthesis.[5,6,11−16] Hence, (i) the 6-substituted pyrrolo[2,3-*d*]pyrimidine ring system, (ii) a thienoyl-for-benzoyl B ring replacement, and (iii) optimal spacing between the pyrrolo[2,3-*d*]pyrimidine system and the terminal L-glutamate all favored FR and PCFT cellular uptake and GARFTase inhibition, resulting in potent antiproliferative activity.[5,6,11−16]

In this report, we continued our systematic study of structural determinants of cellular uptake by RFC, PCFT, and FRs α and -β. A novel series of classical 6-substituted straight chain pyrrolo-[2,3-*d*]pyrimidine antifolates **3a−d** was designed and synthesized as analogues of **2a** with replacement of the phenyl ring by a linear carbon chain of variable lengths (n = 2−5) with or without the terminal L-glutamate. Our results demonstrate, for the first time, that the presence of the phenyl side chain ring is not essential for binding and cellular uptake by FRs. There is an absolute requirement for a terminal L-glutamate, and there is an optimal distance for the alkyl linker separating the pyrrolo[2,3-*d*]pyrimidine ring system and the L-glutamate moiety. The lack of a requirement of the phenyl side chain for FR-mediated cellular uptake is consistent with structural data for FRα[23] and our docking results with compound **3c** and FRα, which show that this region of the molecule interacts with FRα only via hydrophobic interactions.

There were modest differences in surface binding to FRα and -β at neutral pH between the active analogues, **3b−d**, with binding to FRα exceeding that for FRβ. However, this did not translate into corresponding differences in in vitro drug efficacies toward isogenic CHO cell line models expressing one or the other transport system. Rather, inhibition of proliferation of FRβ-expressing CHO cells exceeded that for FRα-expressing CHO cells. This apparent discrepancy may reflect differences in relative affinities of bound substrates at the acidic pH conditions of the endosome for FR α and -β. FRβ but not FRα was found to show (by isothermal titration calorimetry) a pH-dependent decrease in binding affinities for number of classic antifolates (MTX, aminopterin, PMX) at acidic versus neutral pH.[24] By analogy, for the linear 6-substituted pyrrolo[2,3-*d*]pyrimidine

analogues, in spite of their slightly decreased binding affinities for FRβ at pH 7.4, bound drugs may be more effectively released in the endosome than drugs bound to FRα.

For both FRα and -β, the most active compounds of the present series, compounds **3c** and **3d**, bound with the highest affinities and inhibited proliferation of FR-expressing CHO and KB tumor cells with nanomolar potencies approaching those of compounds **2a** and **2b**, among the most potent 6-substituted pyrrolo[2,3-*d*]pyrimidine analogues previously reported by us,[5,11] albeit without any evidence of PCFT transport. Likewise, there was no indication of RFC membrane transport, as an engineered CHO cell line expressing ample human RFC and established in vitro cytotoxicities to RFC antifolate substrates was completely unaffected by the most potent non-benzoyl analogues.

Our results establish that although the phenyl side chain is not essential for FR binding and cellular uptake, it appears to be absolutely necessary for PCFT transport. Inhibition of cell proliferation was attributable to potent inhibition of GARFTase in de novo purine nucleotide bioynthesis at concentrations approximating those which inhibited cell proliferation. Thus, our results are entirely consistent with previous reports that the absence of a side chain phenyl ring in a series of non-benzoyl analogues of LMTX analogues preserved substantial catalytic activity for FPGS and inhibition of isolated GARFTase.[19,20] The structural simplicity and extraordinary antitumor activities of the 6-substituted straight chain compounds described herein provide an excellent starting point for future rational design efforts to further optimize selective cellular uptake by FRs and GARFTase inhibition as an important step toward discovering additional potent targeted antitumor agents.

EXPERIMENTAL SECTION

All evaporations were carried out in vacuo with a rotary evaporator. Analytical samples were dried in vacuo (0.2 mmHg) in a CHEM-DRY drying apparatus over P_2O_5 at 80 °C. Melting points were determined on a MEL-TEMP II melting point apparatus with a FLUKE 51 K/J electronic thermometer and are uncorrected. Nuclear magnetic resonance spectra for proton (^{1}H NMR) were recorded on either a Bruker WH-400 (400 MHz) spectrometer or a Bruker WH-500 (500 MHz) spectrometer. The chemical shift values are expressed in ppm (parts per million) relative to tetramethylsilane as an internal standard: s, singlet; d, doublet; t, triplet; q, quartet; m, multiplet; br, broad singlet. Mass spectra were recorded on a VG-7070 double-focusing mass spectrometer or in a LKB-9000 instrument in the electron ionization (EI) mode. Chemical names follow IUPAC nomenclature. Thin-layer chromatography (TLC) was performed on Whatman Sil G/UV254 silica gel plates with a fluorescent indicator, and the spots were visualized under 254 and 365 nm illumination. All analytical samples were homogeneous on TLC in three different solvent systems. Proportions of solvents used for TLC are by volume. Column chromatography was performed on a 230−400 mesh silica gel (Fisher, Somerville, NJ) column. Elemental analyses were performed by Atlantic Microlab, Inc., Norcross, GA. Element compositions are within 0.4% of the calculated values. Fractional moles of water frequently found in the analytical sample of antifolates could not be prevented in spite of 24−48 h of drying in vacuo and were confirmed where possible by the presence in the ^{1}H NMR spectra. All solvents and chemicals were purchased from Aldrich Chemical Co. or Fisher Scientific and were used as received. For all the compounds submitted for biological evaluation, elemental analysis (C, H, N) was performed to confirm >95% purity.

Ethyl 8-Bromo-7-oxooctanoate (5a). To a solution of 7-methoxy-7-oxoheptanoic acid (**4a**) (0.32 g, 1.5 mmol) in a 50 mL flask was added oxalyl chloride (1.5 mL) and anhydrous CH_2Cl_2 (10 mL). The resulting solution was refluxed for 1 h and then cooled to room temperature. After evaporation of solvent under reduced pressure, the residue was dissolved in ethyl ether (20 mL). The resulting solution was added dropwise to an ice-cold ether solution of diazomethane (generated in situ from 1.4 g *N*-nitroso-*N*-methylurea) over 10 min. To this solution was added 48% HBr (1.5 mL). The resulting mixture was refluxed for 1.5 h. After the mixture was cooled to room temperature, the organic layer was separated and the aqueous layer was extracted with ethyl ether (20 mL × 3). The combined organic layers were washed with two portions of 10% Na_2CO_3 solution and dried over Na_2SO_4. The solvent was evaporated to afford 0.38 g **5a**: yield 79% as white crystals, mp 68−69 °C, R_f = 0.50 (hexane/EtOAc, 5:1). ^{1}H NMR ($CDCl_3$) δ 1.24−1.27 (t, 3 H, CH_3, J = 7.5 Hz), 1.32−1.37 (m, 2 H, CH_2), 1.62−1.65 (m, 4 H, 2 CH_2), 2.28−2.31 (t, 2 H, CH_2, J = 7.5 Hz), 2.65−2.69 (m, 2 H, CH_2), 3.87 (s, 2H, CH_2Br), 4.10−4.14 (q, 2 H, CH_2, J = 7.5 Hz).

Methyl 9-Bromo-8-oxononanoate (5b). Compound **5b** was synthesized as described for **5a**: yield 83% as light-yellow crystals, mp 70−71 °C, R_f = 0.51 (hexane/EtOAc, 5:1). ^{1}H NMR ($CDCl_3$) δ 1.32−1.33 (m, 4 H, 2 CH_2), 1.60−1.63 (m, 4 H, 2 CH_2), 2.28−2.31 (t, 2 H, CH_2, J = 7.5 Hz), 2.63−2.66 (t, 2 H, CH_2, J = 7.5 Hz), 3.66 (s, 3H, CH_3), 3.87 (s, 2H, CH_2Br).

Methyl 10-Bromo-9-oxodecanoate (5c). Compound **5c** was synthesized as described for **5a**: yield 78% as yellow crystals, mp 123−124 °C, R_f = 0.51 (hexane/EtOAc, 5:1). ^{1}H NMR ($CDCl_3$) δ 1.31−1.33 (m, 6 H, 3 CH_2), 1.60−1.62 (m, 4 H, 2 CH_2), 2.28−2.31 (t, 2 H, CH_2, J = 7.5 Hz), 2.63−2.66 (t, 2 H, CH_2, J = 7.5 Hz), 3.66 (s, 3H, CH_3), 3.87 (s, 2H, CH_2Br).

Methyl 11-Bromo-10-oxoundecanoate (5d). Compound **5d** was synthesized as described for **5a**: yield 72% as yellow crystals, mp 92−93 °C, R_f = 0.52 (hexane/EtOAc, 3:1). ^{1}H NMR ($CDCl_3$) δ 1.31−1.33 (m, 8 H, 4 CH_2), 1.59−1.62 (m, 4 H, 2 CH_2), 2.28−2.31 (t, 2 H, CH_2, J = 7.5 Hz), 2.62−2.65 (t, 2 H, CH_2, J = 7.5 Hz), 3.66 (s, 3H, CH_3), 3.87 (s, 2H, CH_2Br).

Ethyl 6-(2-Amino-4-oxo-4,7-dihydro-3*H*-pyrrolo[2,3-*d*]-pyrimidin-6-yl)hexanoate (7a). To a suspension of 2,4-diamino-6-hydroxypyrimidine **6** (1.26 g, 10.0 mmol) in anhydrous DMF (40 mL) was added **5a** (2.64 g, 10.0 mmol). The resulting mixture was stirred under N_2 at room temperature for 3 days. TLC showed the disappearance of starting materials and the formation of one major spot. After evaporation of solvent, CH_3OH (20 mL) was added followed by silica gel (5 g). Evaporation of the solvent afforded a plug, which was loaded onto a silica gel column (3.5 cm × 15 cm) and eluted initially with $CHCl_3$ followed by 10% MeOH in $CHCl_3$ and then 15% MeOH in $CHCl_3$. Fractions showing R_f = 0.39 were pooled and evaporated to afford 1.20 g **7a**: yield 41% as a yellow solid, mp 189−190 °C, R_f = 0.39 ($CHCl_3$/MeOH, 5:1). ^{1}H NMR (DMSO-d_6) δ 1.15−1.17 (t, 3 H, CH_3, J = 7.5 Hz), 1.26−1.31 (m, 2 H, CH_2), 1.52−1.57 (m, 4 H, 2 CH_2), 2.25−2.28 (t, 2 H, CH_2, J = 7.5 Hz), 2.44−2.47 (t, 2 H, CH_2, J = 7.5 Hz), 4.01−4.06 (m, 2 H, OCH_2), 5.84 (s, 1 H, CH), 5.94 (s, 2 H, 2-NH_2), 10.10 (s, 1 H, 3-NH), 10.77 (s, 1H, 7-NH).

Methyl 7-(2-Amino-4-oxo-4,7-dihydro-3*H*-pyrrolo[2,3-*d*]-pyrimidin-6-yl)heptanoate (7b). Compound **7b** was synthesized as described for **7a**: yield 39% as a yellow solid, mp 178−179 °C, R_f = 0.39 ($CHCl_3$/MeOH, 5:1). ^{1}H NMR (DMSO-d_6) δ 1.24−1.29 (m, 4 H, 2 CH_2), 1.49−1.56 (m, 4 H, 2 CH_2), 2.27−2.30 (t, 2 H, CH_2, J = 7.5 Hz), 2.44−2.47 (m, 2 H, CH_2), 3.57 (s, 3 H, OCH_3), 5.83 (s, 1 H, CH), 5.94 (s, 2 H, 2-NH_2), 10.11 (s, 1 H, 3-NH), 10.77 (s, 1H, 7-NH).

Methyl 8-(2-Amino-4-oxo-4,7-dihydro-3*H*-pyrrolo[2,3-*d*]-pyrimidin-6-yl)octanoate (7c). Compound **7c** was synthesized as described for **7a**: yield 43% as a yellow solid, mp 162−163 °C, R_f = 0.41 ($CHCl_3$/MeOH, 5:1). ^{1}H NMR (DMSO-d_6) δ 1.21−1.30 (m, 6 H, 3 CH_2), 1.49−1.56 (m, 4 H, 2 CH_2), 2.27−2.29 (t, 2 H, CH_2, J = 7.5 Hz), 2.43−2.47 (t, 2 H, CH_2, J = 7.5 Hz), 3.57 (s, 3 H, OCH_3), 5.84 (s, 1 H, CH), 6.00 (s, 2 H, 2-NH_2), 10.16 (s, 1 H, 3-NH), 10.79 (s, 1H, 7-NH).

Methyl 9-(2-Amino-4-oxo-4,7-dihydro-3*H*-pyrrolo[2,3-*d*]-pyrimidin-6-yl)nonanoate (7d). Compound **7d** was synthesized as described for **7a**: yield 42% as a yellow solid, mp 165−166 °C, R_f = 0.41 ($CHCl_3$/MeOH, 5:1). ^{1}H NMR (DMSO-d_6) δ 1.21−1.30 (m, 8 H, 4 CH_2), 1.49−1.56 (m, 4 H, 2 CH_2), 2.26−2.29 (t, 2 H, CH_2, J = 7.5 Hz), 2.44−2.47 (t, 2 H, CH_2, J = 7.5 Hz), 3.57 (s, 3 H, OCH_3), 5.85 (s, 1 H, CH), 6.03 (s, 2 H, 2-NH_2), 10.20 (s, 1 H, 3-NH), 10.81 (s, 1H, 7-NH).

6-(2-Amino-4-oxo-4,7-dihydro-3*H*-pyrrolo[2,3-*d*]pyrimidin-6-yl)hexanoic Acid (7e). To a solution of the ester **7a** (100 mg, 0.26 mmol) was added 1N NaOH (5 mL), and the mixture was stirred

dx.doi.org/10.1021/jm401139z | J. Med. Chem. 2013, 56, 8684−8695

under N_2 at room temperature for 1 h. TLC showed the disappearance of the starting material and formation of one major spot at the origin ($CHCl_3$/MeOH, 5:1). The resulting solution was cooled in an ice bath, and the pH was adjusted to 3−4 with dropwise addition of 1N HCl or acetic acid. The resulting suspension was frozen in a dry ice/acetone bath, thawed in a refrigerator to 4−5 °C, and filtered. The residue was washed with a small amount of cold water, dichloromethane, and ethyl acetate and dried in vacuo using P_2O_5 to afford 81 mg **7e**: yield 93% as a yellow powder, mp 188−189 °C decomposed, R_f = 0.06 ($CHCl_3$/MeOH, 5:1). ^{1}H NMR (DMSO-d_6) δ 1.20−1.30 (m, 2 H, CH_2), 1.47−1.56 (m, 4 H, 2 CH_2), 2.17−2.20 (t, 2 H, CH_2, J = 7.5 Hz), 2.43−2.47 (t, 2 H, CH_2, J = 7.5 Hz), 5.83 (s, 1 H, CH), 5.94 (s, 2 H, 2-NH_2), 10.11 (s, 1 H, 3-NH), 10.77 (s, 1H, 7-NH), 11.95 (s, 1H, COOH). Anal. ($C_{12}H_{16}N_4O_3$·0.2 $CH_3COOC_2H_5$·0.2CH_3COOH) C, H, N.

7-(2-Amino-4-oxo-4,7-dihydro-3*H*-pyrrolo[2,3-*d*]pyrimidin-6-yl)heptanoic Acid (7f). Compound **7f** was synthesized as described for **7e**: yield 91% as a brown powder, mp 200−201 °C decomposed, R_f = 0.08 ($CHCl_3$/MeOH, 5:1). ^{1}H NMR (DMSO-d_6) δ 1.20−1.30 (m, 4 H, 2 CH_2), 1.47−1.56 (m, 4 H, 2 CH_2), 2.17−2.20 (t, 2 H, CH_2, J = 7.5 Hz), 2.44−2.47 (t, 2 H, CH_2, J = 7.5 Hz), 5.83 (s, 1 H, CH), 5.94 (s, 2 H, 2-NH_2), 10.11 (s, 1 H, 3-NH), 10.77 (s, 1H, 7-NH), 11.95 (s, 1H, COOH). Anal. ($C_{13}H_{18}N_4O_3$·0.6CH_3OH) C, H, N.

8-(2-Amino-4-oxo-4,7-dihydro-3*H*-pyrrolo[2,3-*d*]pyrimidin-6-yl)octanoic Acid (7g). Compound **7g** was synthesized as described for **7e**: yield 89% as a brown powder, mp 211−212 °C decomposed, R_f = 0.06 ($CHCl_3$/MeOH, 5:1). ^{1}H NMR (DMSO-d_6) δ 1.20−1.30 (m, 6 H, 3 CH_2), 1.47−1.56 (m, 4 H, 2 CH_2), 2.17−2.20 (t, 2 H, CH_2, J = 7.5 Hz), 2.43−2.47 (t, 2 H, CH_2, J = 7.5 Hz), 5.83 (s, 1 H, CH), 5.94 (s, 2 H, 2-NH_2), 10.10 (s, 1 H, 3-NH), 10.76 (s, 1H, 7-NH), 11.94 (s, 1H, COOH). Anal. ($C_{14}H_{20}N_4O_3$·0.4H_2O) C, H, N.

9-(2-Amino-4-oxo-4,7-dihydro-3*H*-pyrrolo[2,3-*d*]pyrimidin-6-yl)nonanoic Acid (7h). Compound **7h** was synthesized as described for **7e**: yield 95% as a brown powder, mp 186 °C decomposed, R_f = 0.09 ($CHCl_3$/MeOH, 5:1). ^{1}H NMR (DMSO-d_6) δ 1.20−1.30 (m, 8 H, 4 CH_2), 1.45−1.56 (m, 4 H, 2 CH_2), 2.17−2.20 (t, 2 H, CH_2, J = 7.5 Hz), 2.44−2.47 (t, 2 H, CH_2, J = 7.5 Hz), 5.83 (s, 1 H, CH), 5.97 (s, 2 H, 2-NH_2), 10.13 (s, 1 H, 3-NH), 10.77 (s, 1H, 7-NH), 11.95 (s, 1H, COOH). Anal. ($C_{15}H_{22}N_4O_3$·0.46CH_2Cl_2) C, H, N.

(*S*)-Diethyl 2-(6-(2-Amino-4-oxo-4,7-dihydro-3*H*-pyrrolo[2,3-*d*]pyrimidin-6-yl)hexanamido)pentanedioate (8a). To a suspension of **7e** (81 mg, 0.34 mmol) in anhydrous DMF (5 mL) was added 6-chloro-2,4-dimethoxy-1,3,5-triazine (72 mg, 0.42 mmol) and *N*-methylmorpholine (43 mg, 0.42 mmol). After the mixture was stirred at rt for 2 h, *N*-methylmorpholine (43 mg, 0.42 mmol) and diethyl L-glutamate hydrochloride (120 mg, 0.51 mmol) were added all at once. The mixture was stirred at rt for 4 h. TLC showed the formation of one major spot at R_f = 0.62 ($CHCl_3$/MeOH, 5:1). The reaction mixture was evaporated to dryness under reduced pressure. The residue was dissolved in a minimum amount of $CHCl_3$/MeOH, 5:1 and chromatographed on a silica gel column (2 cm ×15 cm) with 4% MeOH in $CHCl_3$ as the eluent. Fractions that showed the desired single spot at R_f = 0.62 were pooled and evaporated to dryness to afford **8a** 102 mg: yield 67% as a yellow syrup, R_f = 0.62 ($CHCl_3$/MeOH, 5:1). ^{1}H NMR (DMSO-d_6) δ 1.15−1.18 (t, 6 H, 2 CH_3, J = 7.0 Hz), 1.23−1.29 (m, 2 H, CH_2), 1.48−1.58 (m, 4 H, 2 CH_2), 1.76−1.82 (m, 1 H, CH), 1.92−1.98 (m, 1 H, CH), 2.09−2.12 (t, 2 H, CH_2, J = 7.0 Hz), 2.33−2.37 (m, 2 H, CH_2), 2.44−2.47 (m, 2 H, CH_2), 4.02−4.07 (m, 4 H, 2 CH_2), 4.19−4.24 (m, 1 H, CH), 5.84 (s, 1 H, CH), 5.94 (s, 2 H, 2-NH_2), 8.16 (d, 1 H, CONH, J = 3.8 Hz), 10.10 (s, 1 H, 3-NH), 10.76 (s, 1H, 7-NH).

(*S*)-Diethyl 2-(7-(2-amino-4-oxo-4,7-dihydro-3*H*-pyrrolo[2,3-*d*]pyrimidin-6-yl)heptanamido)pentanedioate (8b). Compound **8b** was synthesized as described for **8a**: yield 70% as a yellow syrup, R_f = 0.62 ($CHCl_3$/MeOH, 5:1). ^{1}H NMR (DMSO-d_6) δ 1.15−1.18 (m, 6 H, 2 CH_3), 1.23−1.30 (m, 4 H, 2 CH_2), 1.48−1.58 (m, 4 H, 2 CH_2), 1.76−1.82 (m, 1 H, CH), 1.92−1.99 (m, 1 H, CH), 2.09−2.12 (t, 2 H, CH_2, J = 7.0 Hz), 2.33−2.37 (m, 2 H, CH_2), 2.44−2.47 (m, 2 H, CH_2), 4.02−4.08 (m, 4 H, 2 CH_2), 4.20−4.24 (m, 1 H, CH), 5.83 (s, 1 H, CH), 5.93 (s, 2 H, 2-NH_2), 8.15 (d, 1 H, CONH, J = 3.8 Hz), 10.10 (s, 1 H, 3-NH), 10.77 (s, 1H, 7-NH).

(*S*)-Diethyl 2-(8-(2-Amino-4-oxo-4,7-dihydro-3*H*-pyrrolo[2,3-*d*]pyrimidin-6-yl)octanamido)pentanedioate (8c). Compound **8c** was synthesized as described for **8a**: yield 68% as a yellow syrup, R_f = 0.64 ($CHCl_3$/MeOH, 5:1). ^{1}H NMR (DMSO-d_6) δ 1.16−1.19 (t, 6 H, 2 CH_3, J = 7.0 Hz), 1.22−1.32 (m, 6 H, 3 CH_2), 1.47−1.57 (m, 4 H, 2 CH_2), 1.76−1.82 (m, 1 H, CH), 1.92−1.99 (m, 1 H, CH), 2.09−2.12 (t, 2 H, CH_2, J = 7.0 Hz), 2.34−2.37 (m, 2 H, CH_2), 2.45−2.48 (m, 2 H, CH_2), 4.02−4.08 (m, 4 H, 2 CH_2), 4.20−4.24 (m, 1 H, CH), 5.84 (s, 1 H, CH), 5.94 (s, 2 H, 2-NH_2), 8.15 (d, 1 H, CONH, J = 3.8 Hz), 10.10 (s, 1 H, 3-NH), 10.76 (s, 1H, 7-NH).

(*S*)-Diethyl 2-(9-(2-Amino-4-oxo-4,7-dihydro-3*H*-pyrrolo[2,3-*d*]pyrimidin-6-yl)nonanamido)pentanedioate (8d). Compound **8d** was synthesized as described for **8a**: yield 66% as a yellow syrup, R_f = 0.64 ($CHCl_3$/MeOH, 5:1). ^{1}H NMR (DMSO-d_6) δ 1.15−1.18 (t, 6 H, 2 CH_3, J = 7.0 Hz), 1.22−1.32 (m, 8 H, 4 CH_2), 1.47−1.57 (m, 4 H, 2 CH_2), 1.76−1.82 (m, 1 H, CH), 1.92−1.99 (m, 1 H, CH), 2.09−2.12 (t, 2 H, CH_2, J = 7.0 Hz), 2.34−2.37 (m, 2 H, CH_2), 2.45−2.48 (m, 2 H, CH_2), 4.02−4.08 (m, 4 H, 2 CH_2), 4.20−4.24 (m, 1 H, CH), 5.83 (s, 1 H, CH), 5.94 (s, 2 H, 2-NH_2), 8.15 (d, 1 H, CONH, J = 3.8 Hz), 10.10 (s, 1 H, 3-NH), 10.77 (s, 1H, 7-NH).

(*S*)-2-(6-(2-Amino-4-oxo-4,7-dihydro-3*H*-pyrrolo[2,3-*d*]-pyrimidin-6-yl)hexanamido)pentanedioic Acid (3a). To a solution of the diester **8a** (100 mg, 0.22 mmol) was added 1N NaOH (5 mL), and the mixture was stirred under N_2 at room temperature for 1 h. TLC showed the disappearance of the starting material and formation of one major spot at the origin ($CHCl_3$/MeOH, 5:1). The resulting solution was cooled in an ice bath, and the pH was adjusted to 3−4 with dropwise addition of 1N HCl. The resulting suspension was frozen in a dry ice/acetone bath, thawed in a refrigerator to 4−5 °C, and filtered. The residue was washed with a small amount of cold water and ethyl acetate and dried in vacuo using P_2O_5 to afford 78 mg **3a**: yield 90% as a white powder, mp 145−146 °C decomposed, R_f = 0.08 ($CHCl_3$/MeOH, 5:1). ^{1}H NMR (DMSO-d_6) δ 1.24−1.30 (m, 2 H, CH_2), 1.48−1.58 (m, 4 H, 2 CH_2), 1.71−1.79 (m, 1 H, CH), 1.88−1.95 (m, 1 H, CH), 2.09−2.12 (t, 2 H, CH_2, J = 7.5 Hz), 2.24−2.27 (m, 2 H, CH_2, J = 7.5 Hz), 2.44−2.47 (m, 2 H, CH_2), 4.16−4.21 (m, 1 H, CH), 5.84 (s, 1 H, CH), 5.95 (s, 2 H, 2-NH_2), 7.99 (d, 1 H, CONH, J = 4.0 Hz), 10.10 (s, 1 H, 3-NH), 10.76 (s, 1H, 7-NH), 12.50 (br, 2 H, 2 COOH). Anal. ($C_{17}H_{23}N_5O_6$·2.0H_2O) C, H, N.

(*S*)-2-(7-(2-Amino-4-oxo-4,7-dihydro-3*H*-pyrrolo[2,3-*d*]-pyrimidin-6-yl)heptanamido)pentanedioic Acid (3b). Compound **3b** was synthesized as described for **3a**: yield 91% as a pale-yellow powder, mp 116−117 °C decomposed, R_f = 0.08 ($CHCl_3$/MeOH, 5:1). ^{1}H NMR (DMSO-d_6) δ 1.22−1.32 (m, 4 H, 2 CH_2), 1.45−1.58 (m, 4 H, 2 CH_2), 1.71−1.79 (m, 1 H, CH), 1.91−1.98 (m, 1 H, CH), 2.09−2.12 (t, 2 H, CH_2, J = 7.5 Hz), 2.24−2.28 (m, 2 H, CH_2, J = 7.5 Hz), 2.44−2.47 (m, 2 H, CH_2), 4.16−4.21 (m, 1 H, CH), 5.84 (s, 1 H, CH), 5.94 (s, 2 H, 2-NH_2), 8.02 (d, 1 H, CONH, J = 4.0 Hz), 10.10 (s, 1 H, 3-NH), 10.76 (s, 1H, 7-NH), 12.12 (br, 1 H, 1 COOH), 12.52 (br, 1 H, 1 COOH). Anal. ($C_{18}H_{25}N_5O_6$·0.5H_2O) C, H, N.

(*S*)-2-(8-(2-Amino-4-oxo-4,7-dihydro-3*H*-pyrrolo[2,3-*d*]-pyrimidin-6-yl)octanamido)pentanedioic Acid (3c). Compound **3c** was synthesized as described for **3a**: yield 95% as a yellow powder, mp 135−136 °C decomposed, R_f = 0.08 ($CHCl_3$/MeOH, 5:1). ^{1}H NMR (DMSO-d_6) δ 1.20−1.32 (m, 6 H, 3 CH_2), 1.45−1.58 (m, 4 H, 2 CH_2), 1.71−1.79 (m, 1 H, CH), 1.90−1.98 (m, 1 H, CH), 2.08−2.12 (t, 2 H, CH_2, J = 7.5 Hz), 2.24−2.28 (m, 2 H, CH_2, J = 7.5 Hz), 2.44−2.47 (t, 2 H, CH_2, J = 7.5 Hz), 4.16−4.21 (m, 1 H, CH), 5.84 (s, 1 H, CH), 5.94 (s, 2 H, 2-NH_2), 8.02 (d, 1 H, CONH, J = 3.8 Hz), 10.11 (s, 1 H, 3-NH), 10.76 (s, 1H, 7-NH). Anal. ($C_{19}H_{27}N_5O_6$·0.5H_2O) C, H, N.

(*S*)-2-(9-(2-Amino-4-oxo-4,7-dihydro-3*H*-pyrrolo[2,3-*d*]-pyrimidin-6-yl)nonanamido)pentanedioic Acid (3d). Compound **3d** was synthesized as described for **3a**: yield 90% as a pale-yellow powder, mp 123−124 °C, decomposed, R_f = 0.08 ($CHCl_3$/MeOH, 5:1). ^{1}H NMR (DMSO-d_6) δ 1.20−1.32 (m, 8 H, 4 CH_2), 1.42−1.58 (m, 4 H, 2 CH_2), 1.71−1.79 (m, 1 H, CH), 1.90−1.98 (m, 1 H, CH), 2.08−2.11 (t, 2 H, CH_2, J = 7.5 Hz), 2.24−2.28 (m, 2 H, CH_2, J = 7.5 Hz), 2.44−2.47 (t, 2 H, CH_2, J = 7.5 Hz), 4.16−4.21 (m, 1 H, CH), 5.84 (s, 1 H, CH), 5.94 (s, 2 H, 2-NH_2), 8.01 (d, 1 H, CONH, J = 3.8 Hz), 10.11 (s, 1 H, 3-NH), 10.76 (s, 1H, 7-NH). Anal. ($C_{20}H_{29}N_5O_6$·0.5 H_2O) C, H, N.

Molecular Modeling and Computational Studies. The X-ray crystal structure of human GARFTase at 1.98 Å resolution (PDB ID: 1NJS)[22] was obtained from the protein database. The human GARFTase crystal structure contains GARFTase complexed with the hydrolyzed form of 10-trifluoroacetyl-5,10-dideaza-acyclic-5,6,7,8-tetrahydrofolic acid (10-CF_3CO-DDACTHF). Molecular modeling studies with FRα were carried out using the 2.80 Å crystal structure of human FRα cocrystallized with folic acid (PDB: 4LRH).[23]

Docking studies were performed using LeadIT 2.1.3.[25] The protonation state of the proteins and the ligands were calculated using the default settings. Water molecules in the active site were permitted to rotate freely. The active site was defined by a sphere of 6.5 Å from the native ligand in the crystal structure. Ligands for docking were built using the molecule builder function in MOE 2010.10[26] and energy minimized using the MMF94X forcefield to a constant of 0.05 kcal/mol. Triangle matching was used as the placement method, and the docked poses were scored using default settings. The docked poses were exported and visualized in MOE.

To validate the docking software for docking the proposed compounds, the native ligands for GARFTase (10-CF_3CO-DDACTHF) and FRα (folic acid) were built using the molecule builder function in MOE, energy minimized and docked using LeadIT 2.1.3 as described above. RMSDs of the docked poses were calculated using an SVL code obtained from the MOE web site (www.chemcomp.com) and compared to the conformation of the crystal structure ligands. The best docked pose for 10-CF_3CO-DDACTHF in the human GARFTase crystal structure had an RMSD of 1.0437 Å (docking score: −40.0853), while the best docked pose for FRα had an RMSD of 0.633 Å (docking score: −55.5940). Thus, LeadIT 2.1.3 was validated for our docking purposes in GARFTase and FRα.

Reagents for Biological Studies. [3′,5′,7,9-^{3}H]Folic acid (25 Ci/mmol) and [^{14}C(U)]glycine (87mCi/mmol) were purchased from Moravek Biochemicals (Brea, CA). Unlabeled folic acid was purchased from Sigma Chemical Co. (St. Louis, MO). LCV [(6*R*,*S*)-5-formyl tetrahydrofolate] was provided by the Drug Development Branch, National Cancer Institute, Bethesda, MD. The sources of the classical antifolate drugs were as follows: MTX, Drug Development Branch, National Cancer Institute (Bethesda, MD); RTX [*N*-(5-[*N*-(3,4-dihydro-2-methyl-4-oxyquinazolin-6-ylmethyl)-*N*-methyl-amino]-2-thienoyl)-L-glutamic acid], AstraZeneca Pharmaceuticals (Maccesfield, Cheshire, England); PDX ((2*S*)-2-[[4-[(1*RS*)-1-[(2, 4-diaminopteridin-6-yl)methyl]but-3-ynyl]benzoyl]amino]pentanedioic acid), Allos Therapeutics (Henderson, NV); and LMTX (5,10-dideaza-5,6,7,8-tetrahydrofolate) and PMX [*N*-{4-[2-(2-amino-3,4-dihydro-4-oxo-7*H*-pyrrolo[2,3-*d*]pyrimidin-5-yl)ethyl]benzoyl}-L-glutamic acid] (Alimta), Eli Lilly and Co. (Indianapolis, IN). Other chemicals were obtained from commercial sources in the highest available purity.

Cell Lines and Assays of Antitumor Drug Activities. The origin of the engineered CHO cell lines, including the RFC-, PCFT-, and FRα-null MTXRIIOua^{R}2−4 (R2), and RFC- (pC43-10), PCFT- (R2/PCFT4), or FRα- (RT16) expressing sublines, were previously described.[11,12,21] Likewise, pDNA3.1 vector control CHO cells (R2/VC) were reported.[11,12] The CHO cells were cultured in α-minimal essential medium (MEM) supplemented with 10% bovine calf serum (Invitrogen, Carlsbad, CA), 100 units/ml penicillin/100 μg/mL streptomycin, and 2 mM L-glutamine at 37 °C with 5% CO_2. All the R2 transfected cells [PC43-10, RT16, R2/hPCFT4, R2(VC)] were routinely cultured in α-MEM plus 1.5 mg/mL G418. Prior to the cell proliferation assays (see below), RT16 cells were cultured in complete folate-free RPMI 1640 (without added folate) for three days. R2/hPCFT4 and R2(VC) cells were cultured in complete folate-free RPMI 1640 including dFBS (Invitrogen) and 25 nM LCV with 1.5 mg/mL G418. KB human nasopharyngeal carcinoma cells were purchased from the American Type Culture Collection (Manassas, VA). KB cells were routinely cultured in folate-free RPMI 1640 medium, supplemented with 10% fetal bovine serum, penicillin−streptomycin solution, and 2 mM L-glutamine at 37 °C with 5% CO_2.

For growth inhibition assays, cells (CHO and KB) were plated in 96 well dishes (~2500−5000 cells/well, total volume of 200 μL medium) with a range of antifolate concentrations.[11−16] The medium was RPMI 1640 (contains 2.3 μM folic acid) with 10% dFBS and antibiotics for experiments with R2 and PC43-10 cells. For RT16 and KB cells, cells were cultured in folate-free RPMI media with 10% dFBS and antibiotics supplemented with 2 nM LCV and 2 mM L-glutamine. The requirement for FR-mediated drug uptake in these assays was established in parallel incubations including 200 nM folic acid. For R2/hPCFT4 cells, the medium was folate-free RPMI 1640 (pH 7.2) containing 25 nM LCV, supplemented with 10% dFBS, antibiotics, and L-glutamine. Cells were routinely incubated for up to 96 h, and metabolically active cells (a measure of cell viability) were assayed with CellTiter-blue cell viability assay (Promega, Madison, WI), with fluorescence measured (590 nm emission, 560 nm excitation) using a fluorescence plate reader.[11−16] Raw data were exported from Softmax Pro software to an Excel spreadsheet for analysis and determinations of IC_{50}s, corresponding to the drug concentrations that result in 50% loss of cell growth.[11−16]

For some of the in vitro growth inhibition studies, the inhibitory effects of the antifolate inhibitors on de novo thymidylate biosynthesis (i.e., thymidylate synthase) and de novo purine nucleotide biosynthesis (GARFTase and AICARFTase) were tested by coincubations with thymidine (10 μM) and adenosine (60 μM), respectively.[11−17] For de novo purine nucleotide biosynthesis, additional protection experiments used AICA (320 μM) to distinguish inhibitory effects at GARFTase from those at AICARFTase.[11−17]

FR Binding Assay. Competitive inhibition of [^{3}H]folic acid binding to FRα and FRβ using RT16 and D4 CHO cells, respectively, was used was used to assess relative binding affinities for assorted (anti)folate ligands.[11,12,14−16] For these experiments, cells (~1.6×10^6) were rinsed twice with DPBS, followed by two washes an acidic buffer (10 mM sodium acetate, 150 mM NaCl, pH 3.5) to remove FR-bound folates. Cells were washed twice with ice-cold HEPES-buffered saline (20 mM HEPES, 140 mM NaCl, 5 mM KCl, 2 mM $MgCl_2$, 5 mM glucose, pH 7.4) (HBS), then incubated in HBS with [^{3}H]folic acid (50 nM, specific activity 0.5 Ci/mmol) in the presence and absence of unlabeled folic acid or antifolates (over a range of concentrations) for 15 min at 0 °C. The dishes were rinsed three times with ice-cold HBS, after which the cells were solubilized (0.5 N NaOH) and aliquots measured for radioactivity and protein contents. Protein concentrations were measured with Folin phenol reagent.[27] [^{3}H]Folic acid bound to FRα and FRβ was calculated as pmol/mg protein, and relative binding affinities were calculated in each individual experiment as the inverse molar ratios of unlabeled ligands required to inhibit [^{3}H]folic acid binding by 50%.[11,12,14−16] By definition, the relative affinity of folic acid is 1. Experiments were performed in triplicate.

In Situ GARFT Enzyme Inhibition Assay. Incorporation of [^{14}C]glycine into [^{14}C]formyl GAR, as an in situ measure of endogenous GARFTase activity, was measured.[6,11−17] For these experiments, KB cells were seeded in 4 mL of complete folate-free RPMI 1640 plus 2 nM LCV in 60 mm dishes at a density of 2×10^6 cells per dish. On the next day, the medium was replaced with 2 mL of fresh complete folate-free RPMI 1640 plus 2 nM LCV. Azaserine (4 μM final concentration) was added in the presence and absence of the antifolate inhibitors. After 30 min, L-glutamine (final concentration, 2 mM) and [^{14}C]glycine (tracer amounts; final specific activity 0.1 mCi/L) were added. Incubations were at 37 °C for 15 h, at which time cells were washed (one-time) with ice-cold PBS. Cell pellets were dissolved in 2 mL of 5% trichloroacetic acid at 0 °C. The trichloracetic acid insoluble fraction was removed by centrifugation and solubilized in 0.5N NaOH, and the cell protein contents were measured with Folin phenol reagent.[27] The supernatants were extracted twice with 2 mL of ice-cold ether. The aqueous layer was passed through a 1 cm column of AG1 × 8 (chloride form), 100−200 mesh (Bio-Rad), washed with 10 mL of 0.5N formic acid and then 10 mL of 4N formic acid, and finally eluted with 8 mL of 1N HCl. The eluates were collected and determined for radioactivity. The accumulation of [^{14}C]formyl GAR was calculated as pmol per mg protein over a range of inhibitor concentrations. IC_{50}s were calculated as the concentrations of inhibitors that resulted in a 50% decrease in [^{14}C]formyl GAR synthesis. Experiments were performed in triplicate.

■ ASSOCIATED CONTENT

Supporting Information

Elemental analysis. This material is available free of charge via the Internet at http://pubs.acs.org.

■ AUTHOR INFORMATION

Corresponding Authors

*For L.H.M.: phone, 313-578-4280; fax, 313-578-4287; E-mail, matherly@karmanos.org; address, Molecular Therapeutics Program, Barbara Ann Karmanos Cancer Institute, 110 East Warren Avenue, Detroit, Michigan 48201, United States.

*For A.G.: phone, 412-396-6070; fax, 412-396-5593; E-mail, gangjee@duq.edu; address, Division of Medicinal Chemistry, Graduate School of Pharmaceutical Sciences, Duquesne University, 600 Forbes Avenue, Pittsburgh, Pennsylvania 15282, United States.

Present Address

⊥Center for Drug Discovery and Translational Research, Beth Israel Deaconess Medical Center, Harvard Medical School, Boston Massachusetts 02215, United States. Phone: 617-667-1839. E-mail: ywang15@bidmc.harvard.edu.

Author Contributions

#Y.W. and C.C. contributed equally to this work. L.H.M. and A.G. contributed equally to this work.

Notes

The authors declare no competing financial interest.

■ ACKNOWLEDGMENTS

This work was supported in part by grants from the National Institutes of Health, National Cancer Institute CA152316 (L.H.M. and A.G.), CA166711 (A.G. and L.H.M.), and CA53535 (L.H.M.), and the Duquesne University Adrian Van Kaam Chair in Scholarly Excellence (A.G.). S.M.-R. was supported by T32 CA009531 (L.H.M.) and F31 CA165853 (S.M.-R.).

■ ABBREVIATIONS USED

AICA, 5-aminoimidazole-4-carboxamide; AICARFTase, 5-aminoimidazole-4-carboxamide ribonucleotide formyltransferase; CHO, Chinese hamster ovary; dFBS, dialyzed fetal bovine serum; DPBS, Dulbecco's phosphate-buffered saline; FR, folate receptor; FPGS, folylpolyglutamate synthetase; GAR, glycinamide ribonucleotide; GARFTase, glycinamide ribonucleotide formyltransferase; HBSS, Hank's Balanced Salts Solution; HBS, HEPES-buffered saline; LCV, leucovorin; LMTX, lometrexol; MTX, methotrexate; MEM, minimal essential media; PMX, pemetrexed; PDX, pralatrexate; PCFT, proton-coupled folate transporter; RTX, raltiterxed; RFC, reduced folate carrier; SAR, structure−activity relationship; 10-CF_3CO-DDACTHF, 10-trifluoroacetyl-5,10-dideaza-acyclic-5,6,7,8-tetrahydrofolic acid

■ REFERENCES

(1) Matherly, L. H.; Hou, Z.; Deng, Y. Human Reduced Folate Carrier: Translation of Basic Biology to Cancer Etiology and Therapy. *Cancer Metastasis Rev.* **2007**, *26*, 111−128.

(2) Elnakat, H.; Ratnam, M. Distribution, Functionality and Gene Regulation of Folate Receptor Isoforms: Implications in Targeted Therapy. *Adv. Drug Delivery Rev.* **2004**, *56*, 1067−1084.

(3) Yang, J.; Vlashi, E.; Low, P. Folate-linked Drugs for the Treatment of Cancer and Inflammatory Diseases. *Subcell Biochem.* **2012**, *56*, 163−179.

(4) Zhao, R.; Matherly, L. H.; Goldman, I. D. Membrane Transporters and Folate Homeostasis: Intestinal Absorption and Transport into Systemic Compartments and Tissues. *Expert Rev. Mol. Med.* **2009**, *11*, e4.

(5) Kugel Desmoulin, S.; Hou, Z.; Matherly, L. H.; Gangjee, A. The Human Proton-Coupled Folate Transporter: Biology and Therapeutic Applications to Cancer. *Cancer Biol. Ther.* **2012**, *13* (14), 1−19.

(6) Kugel Desmoulin, S.; Wang, L.; Hales, E.; Polin, L.; White, K.; Kushner, J.; Stout, M.; Hou, Z.; Cherian, C.; Gangjee, A.; Matherly, L. H. Therapeutic Targeting of a Novel 6-Substituted Pyrrolo[2,3-*d*]-pyrimidine Thienoyl Antifolate to Human Solid Tumors Based on Selective Uptake by the Proton-Coupled Folate Transporter. *Mol. Pharmacol.* **2011**, *80*, 1096−1107.

(7) Visentin, M.; Zhao, R.; Goldman, I. D. The Antifolates. *Hematol. Oncol. Clin. North Am.* **2012**, *26*, 629−648.

(8) Gonen, N.; Assaraf, Y. G. Antifolates in Cancer Therapy: Structure, Activity and Mechanisms of Drug Resistance. *Drug Resist. Updates* **2012**, *15*, 183−210.

(9) Sirotnak, F. M.; DeGraw, J. I.; Colwell, W. T.; Piper, J. R. A New Analogue of 10-Deazaaminopterin with Markedly Enhanced Curative Effects Against Human Tumor Xenografts in Mice. *Cancer Chemother. Pharmacol.* **1998**, *42*, 313−318.

(10) Zhao, R.; Goldman, I. D. Resistance To Antifolates. *Oncogene* **2003**, *22*, 7431−7457.

(11) Deng, Y.; Wang, Y.; Cherian, C.; Hou, Z.; Buck, S., A.; Matherly, L. H.; Gangjee, A. Synthesis and Discovery of High Affinity Folate Receptor-Specific Glycinamide Ribonucleotide Formyltransferase Inhibitors with Antitumor Activity. *J. Med. Chem.* **2008**, *51*, 5052−5063.

(12) Deng, Y.; Zhou, X.; Desmoulin, S. K.; Matherly, L. H.; Gangjee, A. Synthesis and Biological Activity of a Novel Series of 6-Substituted Thieno[2,3-*d*]pyrimidine Antifolate Inhibitors of Purine Biosynthesis with Selectivity for High Affinity Folate Receptors over the Reduced Folate Carrier and Proton-Coupled Folate Transporter for Cellular Entry. *J. Med. Chem.* **2009**, *52*, 2940−2951.

(13) Desmoulin, S. K.; Wang, Y.; Matherly, L. H.; Gangjee, A. Targeting the Proton-Coupled Folate Transporter for Selective Delivery of 6-Substituted [2,3-*d*] pyrimidine Antifolate Inhibitors of de Novo Purine Biosynthesis in the Chemotherapy of Solid Tumors. *Mol. Pharmacol.* **2010**, *78*, 577−587.

(14) Wang, L.; Cherian, C.; Desmoulin, S. K.; Polin, L.; Deng, Y.; Wu, J.; Hou, Z.; White, K.; Kushner, J.; Matherly, L. H.; Gangjee, A. Synthesis and Antitumor Activity of a Novel Series of 6-Substituted Pyrrolo[2,3-*d*]pyrimidine Thienoyl Antifolate Inhibitors of Purine Biosynthesis with Selectivity for High Affinity Folate Receptors and the Proton-Coupled Folate Transporter over the Reduced Folate Carrier for Cellular Entry. *J. Med. Chem.* **2010**, *53*, 1301−1318.

(15) Wang, L.; Desmoulin, S. K.; Matherly, L. H.; Gangjee, A. Synthesis, Biological, and Antitumor Activity of a Highly Potent 6-Substituted Pyrrolo[2,3-*d*] pyrimidine Thienoyl Antifolate Inhibitor with Proton-Coupled Folate Transporter and Folate Receptor Selectivity over the Reduced Folate Carrier that Inhibits *β*-Glycinamide Ribonucleotide Formyltransferase. *J. Med. Chem.* **2011**, *54*, 7150−7164.

(16) Wang, L.; Cherian, C.; Desmoulin, S. K.; Matherly, L. H.; Gangjee, A. Synthesis and Biological Activity of 6-Substituted Pyrrolo[2,3-*d*]pyrimidine Thienoyl Regioisomers as Inhibitors of de Novo Purine Biosynthesis with Selectivity for Cellular Uptake by High Affinity Folate Receptors and the Proton-Coupled Folate Transporter over the Reduced Folate Carrier. *J. Med. Chem.* **2012**, *55*, 1758−1770.

(17) Beardsley, G. P.; Moroson, B. A.; Taylor, E. C.; Moran, R. G. A New Antimetabolite, 5,10-Dideaza-5,6,7,8-Tetrahydrofolate is a Potent Inhibitor of de Novo Purine Synthesis. *J. Biol. Chem.* **1989**, *264*, 328−333.

(18) Ray, M. S.; Muggia, F. M.; Leichman, C. G.; Grunberg, S. M.; Nelson, R. L.; Dyke, R. W.; Moran, R. G. Phase I Study of (6*R*)-5,10-Dideazatetrahydrofolate: A Folate Antimetabolite Inhibitory to de Novo Purine Synthesis. *J. Natl. Cancer Inst.* **1993**, *85*, 1154−1159.

(19) Baldwin, S. W.; Tse, A.; Gossett, L. S.; Taylor, E. C.; Rosowsky, A.; Shih, C.; Moran, R. G. Structural Features of 5,10-Dideaza-5,6,7,8-tetrahydrofolate That Determine Inhibition of Mammalian Glycinamide Ribonucleotide Formyltransferase. *Biochemistry* **1991**, *30*, 1997−2006.

(20) Habeck, L. L.; Mendelsohn, L. G.; Shih, C.; Taylor, E. C.; Colman, P. D.; Gossett, L. S.; Leitner, T. A.; Schultz, R. M.; Andis, S. L.; Moran, R. G. Substrate Specificity of Mammalian Folylpoylglutamate Synthetase for 5,10-Dideazatetrahydrofolate Analogs. *Mol. Pharmacol.* **1995**, *48*, 326−333.
(21) Wong, S. C.; Proefke, S. A.; Bhushan, A.; Matherly, L. H. Isolation of Human cDNAs That Restore Methotrexate Sensitivity and Reduced Folate Carrier Activity in Methotrexate Transport-Defective Chinese Hamster Ovary Cells. *J. Biol. Chem.* **1995**, *270*, 17468−17475.
(22) Zhang, Y.; Desharnais, J.; Marsilje, T. H.; Li, C.; Hedrick, M. P.; Gooljarsingh, L. T.; Tavassoli, A.; Benkovic, S. J.; Olson, A. J.; Boger, D. L.; Wilson, I. A. Rational Design, Synthesis, Evaluation, and Crystal Structure of a Potent Inhibitor of Human GAR Tfase: 10-(Trifluoroacetyl)-5,10-dideazaacyclic-5,6,7,8-tetrahydrofolic Acid. *Biochemistry* **2003**, *42*, 6043−6056.
(23) Chen, C.; Ke, J.; Zhou, X. E.; Brunzelle, J. S.; Li, J.; Yong, E.-L.; Xu, H. E.; Melcher, K. Structural Basis For Molecular Recognition of Folic Acid by Folate Receptors. *Nature* **2013**, *500*, 486−489.
(24) Wibowo, A. S.; Singh, M.; Reeder, K. M.; Carter, J. J.; Kovach, A. R.; Meng, W.; Ratnam, M.; Zhang, F.; Dann, C. E., III. Structures of Human Folate Receptors Reveal Biological Trafficking States and Diversity in Folate and Antifolate Recognition. *Proc. Natl. Acad. Sci. U. S. A.* **2013**, *110*, 15180−15188.
(25) *LeadIT 2.1.3*; BioSolveIT GmbH : Sankt Augustin, Germany, 2011.
(26) *MOE 2010.10*; Chemical Computing Group: Montreal, Quebec, Canada, 2010.
(27) Lowry, O. H.; Rosebrough, N. J.; Farr, A. L.; Randall, R. J. Protein Measurement With the Folin Phenol Reagent. *J. Biol. Chem.* **1951**, *193*, 265−275.